INSTITUTE OF PHYSICS PUBLISHING JOURNAL OF PHYSICS D: APPLIED PHYSICS
J. Phys. D: Appl. Phys. **34** (2001) 477–482 www.iop.org/Journals/jd PII: S0022-3727(01)18081-2

Comparison between the different implantation orders in H^+ and He^+ coimplantation

Xinzhong Duo[1], Weili Liu[1], Miao Zhang[1], Lianwei Wang[1], Chenglu Lin[1], M Okuyama[2], M Noda[2], Wing-Yiu Cheung[3], Paul K Chu[4], Peigang Hu[5], S X Wang[6] and L M Wang[6]

[1] Shanghai Institute of Metallurgy, Chinese Academy of Sciences, Shanghai 200050, People's Republic of China
[2] Area of Materials and Device Physics, Department of Physical Science, Graduate School of Engineering Science, Osaka University, 1-3 Machikaneyama-cho, Toyanaka, Osaka 560-8531, Japan
[3] Department of EEE, Chinese University of Hong Kong, New Territory, Hong Kong, People's Republic of China
[4] City University of Hong Kong, Tat Chee Avenue, Kowloon, Hong Kong, People's Republic of China
[5] Applied Ion Beam Physics Laboratory, Fudan University, Shanghai 200433, People's Republic of China
[6] Department of Nuclear Engineering and Radiological Sciences, College of Engineering, University of Michigan, MI 48109-2104, USA

Received 17 October 2000

Abstract
H^+ and He^+ were implanted into single crystals in different orders (H^+ first or He^+ first). Subsequently, the samples were annealed at different temperatures from 200 °C to 450 °C for 1 h. Cross sectional transmission electron microscopy, Rutherford backscattering spectrometry and channelling, elastic recoil detection were employed to characterize the defects and the distribution of H and He in the samples. Furthermore, the positron traps introduced by ion implantation and annealing were characterized by slow positron annihilation spectroscopy. Both orders in the coimplantation of H and He have the ability to decreases the total implantation dose after annealing. No bubbles or voids but cracks and platelets, were observed by cross sectional transmission electron microscopy. The different implantation orders affect the density of interstitial atoms and positron traps.

1. Introduction

Both hydrogen and helium implantation can cause surface exfoliation and blistering after annealing [1–3, 9]. At present, great interest is focused on the smart-cut process (one of the most important steps in Unibond SOI (silicon on insulator) materials fabrication), which is based on the phenomenon of exfoliation and blistering caused by implantation of hydrogen or helium [4]. This process allows SOI wafers to be fabricated more economically and with better quality than competing processes such as SIMOX (separated by implantation oxygen) and BESOI (bonded and etch-back SOI). Gas ion implantation, usually hydrogen, is a necessary step in the smart-cut process. The thin-film separation process is based on the observation that implantation of a high dose of hydrogen induces surface blistering and exfoliation of metal and the semiconductor. Generally, it is considered that the thin-film separation process is proceeded by chemical interaction (bond breaking and internal surface passivation) and physical interaction (gas coalescence, pressure and fracture) of the implanted H^+ in the silicon substrate. It is difficult to isolate the contribution of each component to the overall process. Helium is another kind of gas used in thin-film separation. Helium does not undergo chemical interaction in H^+ implanted silicon substrates, but it undergoes physical interaction just as hydrogen does and even more efficiently [5]. Coimplantation of hydrogen and

0022-3727/01/040477+06$30.00 © 2001 IOP Publishing Ltd Printed in the UK

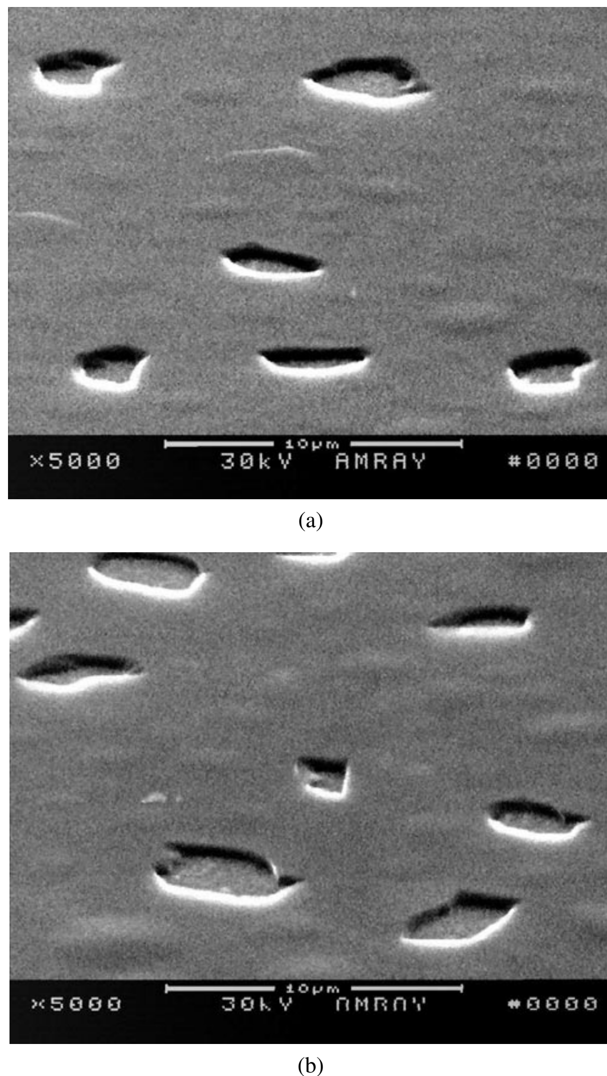

(a)

(b)

Figure 1. SEM micrographs of the surface of samples implanted with (a) hydrogen first and (b) helium first. It can be concluded that the density and size of the craters on the surface of helium-implanted-first samples are slightly higher than those of the hydrogen-implanted-first samples.

helium is a good way to study the different roles of implanted gas ions in implanted samples [6], the interaction between the two kinds of atoms and the correlation between the defects of the H/He atoms. It also helps to decouple the physical and chemical contributions to the blistering and thin-film separation processes. The study of the difference between the different implantation orders will give further understanding of these processes. At the same time, coimplantation requires a much lower total dose of ion implantation than the dose of a single ion implanted alone. This will shorten the implantation time and lighten the crystal damage induced by implantation, which is able to decrease the cost and improve the quality of smart-cut SOI.

In this work, Rutherford backscattering spectrometry and channelling (RBS/C), elastic recoil detect analysis (ERDA), cross sectional transmission electron microscopy (XTEM) and slow positron annihilation spectroscopy (SPAS) were employed to study the coimplanted samples annealed at different temperatures.

2. Experimental details

P-type (5–8 Ω cm) (100) silicon wafers were implanted with H^+ at 30 keV with a dose of 1×10^{16} cm^{-2} and He^+ at 33 keV with a dose of 1×10^{16} cm^{-2} at room temperature in different orders—H^+ first and then He^+ or He^+ first and then H^+. In order to avoid channelling effects, a deliberate misalignment from the wafer normal of 7° was used during implantation. After implantation all wafers were cut into smaller samples for analysis. The samples were given a standard RCA clean prior to analysis to remove any surface contaminants introduced by the implantation. They were then annealed in a temperature range of 200–450 °C for 1 h in the flowing ambient of N_2 gas. The implanted samples were then stored in air at room temperature before measurement.

RBS/C analyses were performed using 2.0 MeV He^+ ions beams. The scattering angle of the RBS spectrum was 140°. In this technique, the backscattering yield is sensitive to the defects in the crystalline matrix. The signal is indeed produced by the silicon atoms unaligned to the channel rows coinciding, in our case, with atoms displaced from their crystalline position in any direction parallel to the surface, especially the interstitial silicon atoms. Rather than the raw RBS data, the profiles of the displacement atoms (or their integral) were calculated according to the algorithm developed in [13]. In the following we shall consider the integral of the displacement atom profile as a quantity proportional to the intensity of the displacement field.

XTEM samples (annealed at 450 °C for an hour) were prepared in the conventional way by mechanical thinning and Ar^+ ion etching. XTEM observation is concerned with the distribution and location of extended defects, bubbles and platelets.

The H and He distributions in the Si samples after implantation and annealing were measured by ERDA, using a 12 MeV $^{16}O^{4+}$ beam (with a cross section of 1×0.3 mm^2) impinging the sample at 75° from the sample normal. The detector was placed at 150° from the beam direction and the forward-scattered oxygen particles were stopped by a 10 μm thick Mylar film. The RUMP program was used to analyse the raw data and calculate the depths and the concentrations of both components.

The profiles of vacancy-type defects were characterized with a slow positron beam. SPAS is highly sensitive to open volume defects as positrons are apt to be trapped and annihilated in sites where the Coulomb core repulsion is a minimum [7, 8]. The positrons were implanted in an energy range of 0.5–15 keV. The Doppler broadening of the 511 keV annihilation γ rays was measured at room temperature. The mean depth z (nm) of the incident positrons is given by $z = (A/\rho)E^n$, where E (keV) is the incident positron energy and ρ (g cm^{-3}) is the mass density of the target. For the Si target, the constants A and n were empirically determined to be 4.0 (μg cm^{-2} keV^{-n}) and 1.6, respectively. The level of the Doppler broadening is indicated by the parameter S, which is defined as the ratio of the counts in a fixed central region ($|511 - E\gamma| < 0.85$ keV) of the 511 keV line to the total counts of the peak ($|511 - E\gamma| < 4.25$ keV.). It should be stressed that vacancy-like defects are active positron traps if they are helium and hydrogen free, however once they are decorated

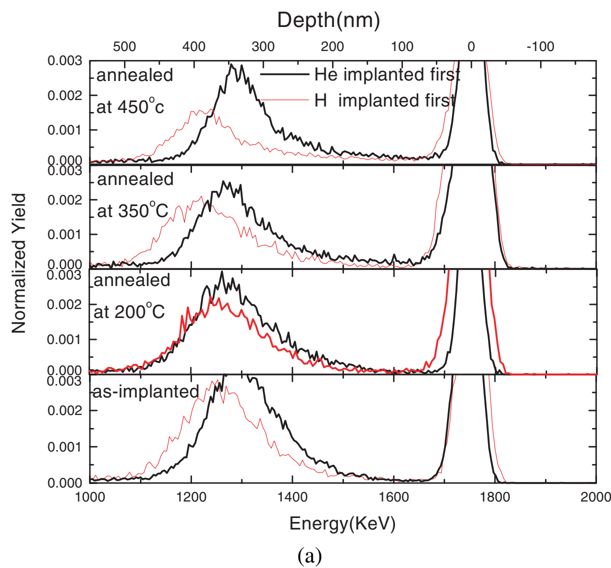

(a)

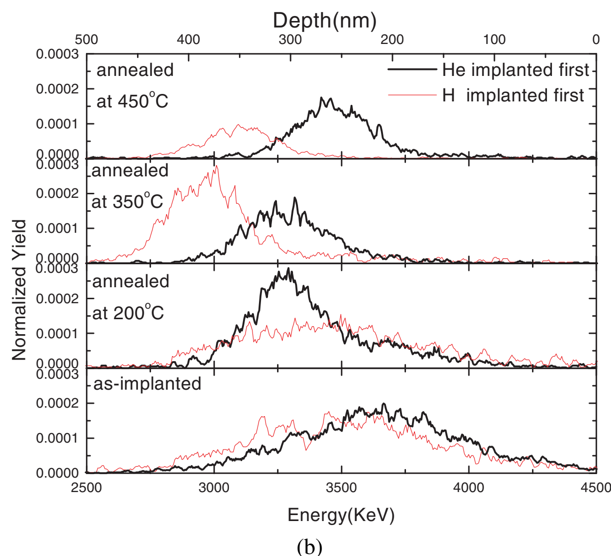

(b)

Figure 2. ERDA yield of different implantation order samples annealed at different temperatures. (a) Distribution of hydrogen. The peak around channel 330 is due to contamination on the surface. The density of hydrogen decreases with the annealing temperature, but the distributions only change a little. (b) Distribution of helium; in the helium-implanted-first samples, the distributions do not move so deep as those in the hydrogen-implanted-first samples. The annealing temperature necessary to move the helium atoms is different for the two kinds of sample.

by helium and hydrogen they become ineffective in trapping positrons. A decrease of the SPAS signal can be due either to trap annealed out or to trap decoration. Conversely, a rise of the SPAS signal can be due to depassivated traps resulting from helium and hydrogen outflow.

3. Results

Based on the observation of optical microscopy and scanning electron microscopy (SEM) (shown in figure 1), the samples implanted in both orders exfoliated after being annealed at 450 °C. The size and density of the craters and blisters on the surface in the helium-implanted-first samples are larger and

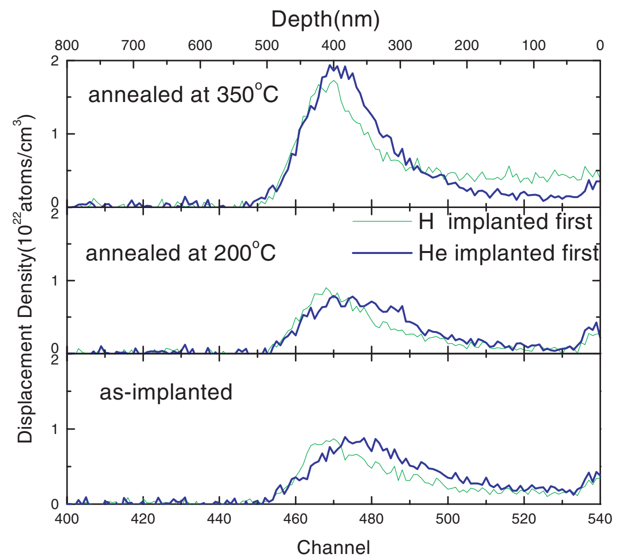

Figure 3. Displacement atom profiles of samples annealed at different temperatures. The density of displacement atoms increase with the annealing temperature and the distribution moves deeper in both kinds of sample. The densities of the displacement atoms are similar when annealed at a lower temperature for both kinds of sample, and is higher in the helium-implanted-first samples after annealing at 350 °C.

higher than those in the hydrogen-implanted-first samples, but the difference is quite small.

To obtain the distributions and the losses of hydrogen and helium in the substrate during annealing, ERDA was employed. The distributions of hydrogen and helium are shown in figures 2(a) and 2(b), respectively. In both implantation orders the samples continuously lose hydrogen during an annealing temperature increase below 450 °C, at which point the samples exfoliate on the surface. In the hydrogen-implanted-first samples, the distribution of hydrogen does not change during annealing below 200 °C, and moves slightly deeper when annealed at 350 °C; while helium accumulates much more sharply, and moves deeper when annealing temperature is over 350 °C. In helium-implanted-first samples, the distribution of hydrogen becomes slightly shallower during annealing, and the distribution of helium becomes deeper, but not so deep as that in hydrogen-implanted-first samples. The hydrogen peaks around the energy of 1750 keV are due to surface contamination. The implantation process was simulated by TRIM96.

On annealing in the temperature range of 200–450 °C, the density of the scattering centre in the implanted region increases greatly. The distribution of damage during ion implantation and the thermal evolution of the defects during annealing were investigated by RBS/C. The channelling spectra of the samples indicate the density of the displacement atoms. When the samples were annealed at 450 °C, the surface was blistered and exfoliated. RBS/C is invalidated under such a situation. A method described in [13] was used to analyse the RBS/C data and characterize the distribution of displacement atoms. The distribution of the displacement atoms against depth are presented in figure 3. The density of the displacement atoms increases with an increase of the annealing temperature, especially in the temperature range

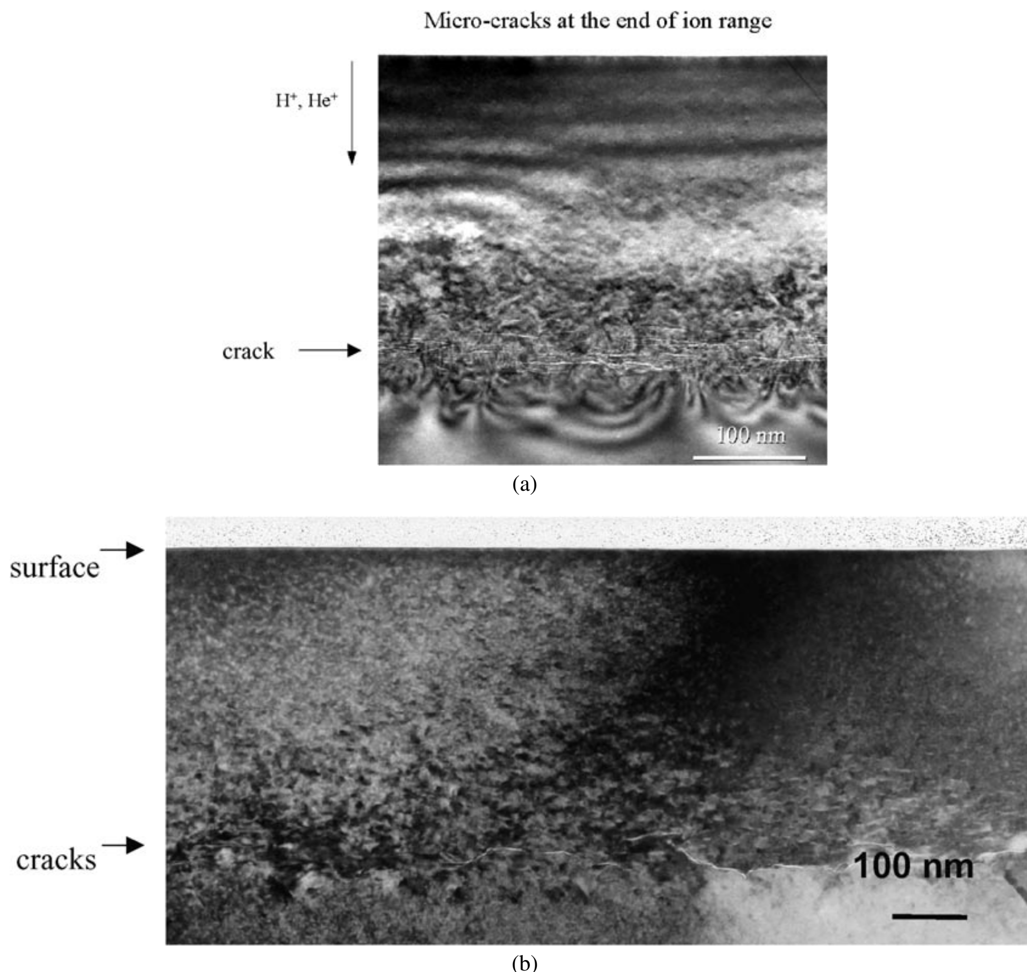

Figure 4. XTEM images of samples annealed at 450 °C for: (a) hydrogen implanted first and (b) helium implanted first. In both samples the depth of the crack is about 400 nm, Most of the platelets are oriented along the (100) plane. The density of platelets is higher in the hydrogen-implanted-first samples.

of 200–350 °C. In the hydrogen-implanted-first samples, the distribution of displacement atoms is a little deeper and the density is a little lower.

XTEM was employed to show the distribution of defects, strain, platelets and bubbles in the samples annealed at 450 °C. In figures 4(a) and 4(b) we can conclude that in both types of sample, a typical electron micrograph of a thinner section reveals that most of the platelets in the defect layer orient along the (100) planes. There are many dislocations and strains distributed near the implanted region, which are induced by stress in the region. It is found that there are a few bubbles near the projected range in the coimplanted samples, while there are many more bubbles in the hydrogen- or helium-only implanted samples. The defect region is quite wide, almost 200 nm, and the depth of the crack is about 400 nm, which is near the implantation depth of hydrogen. The density of cracks is higher in the samples implanted with hydrogen first.

The parameter S for SPAS analysis is low on the surface because positrons diffuse back to the surface. At a high implantation energy most positrons are deep enough to be annihilated far away from the defect region and in all the samples the S value reaches the same asymptotic defect-free value of the material. In the defect region the S value is higher than that in virgin silicon. This difference indicates

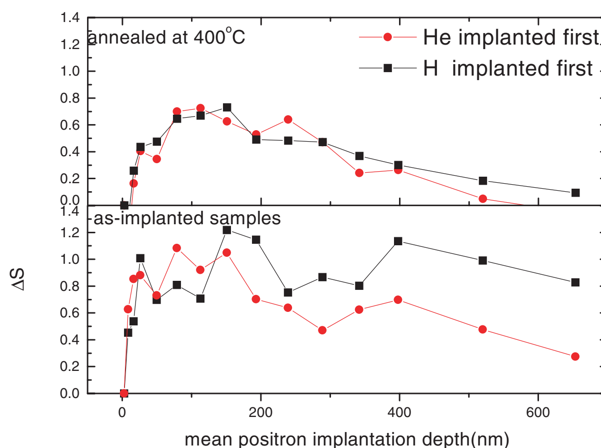

Figure 5. ΔS against mean positron implantation depth for samples annealed at 400 °C and as-implanted samples of the different implantation orders. ΔS is higher in the samples implanted with hydrogen first, especially near the depth of 400 nm.

that an increased fraction of positrons are annihilated with low momentum electrons and is characteristic of positrons trapped in open volume defects.

As discussed in [10], the physical information on the positron traps is well described by the difference of the S parameter of the defect sample minus the corresponding value of the reference sample:

$$\Delta S = \frac{S - S_s}{S_d - S_b} - \frac{S_b - S_s}{S_d - S_b}\left[\frac{S - S_s}{S_b - S_s}\right]_{Virgin\,Si}.$$

Here S_s is the value of the S parameter in the surface layer, S_b is the value of the S parameter in undamaged bulk material and S_d is the value of the S parameter in the damaged region. ΔS against depth is shown in figures 5(a) and 5(b). Based on the analysis, it is very clear that there are two density peaks of the positron trap, one is at 200 nm and the other is at 400 nm. After annealing at 400 °C for 1 h, the deeper peak is almost eliminated and the remainder of this peak moves to 300 nm, the shallower peak also becomes much weaker and move towards the surface, to about 150 nm. It seems that both of the peaks become wider after annealing. Furthermore, in the samples implanted with hydrogen first the density of positron traps is higher, especially the deeper peak.

4. Discussion

The experiment results can be summarized as follows.

(a) Both implantation orders lead to exfoliation of the surface of the samples after annealing at 450 °C. The total implantation dose is lower than the dose that helium- or hydrogen-only single implantation needs ($>4\times10^{16}$ cm^{-2} hydrogen only and $>2\times10^{17}$ cm^{-2} helium only).

(b) In the samples of both implantation orders, some of hydrogen escaped, the remaining hydrogen stays in the implanted position. In hydrogen-implanted-first samples, helium atoms move from their projected range to the hydrogen's projected range during annealing; in helium-implanted-first samples, the helium atoms also move deeper, but their final position is not so deep as than in the hydrogen-implanted-first samples, and is in the middle of their original position and the hydrogen's position.

(c) The RBS/C signals, the signature of silicon interstitial-like defects, increase in density with the increase of the annealing temperature. The densities of the interstitial silicon atoms in samples of different implantation orders are the same when the annealing temperature is lower than 350 °C, but the interstitial silicon atoms densities in the samples implanted with helium first are higher and shallower after being annealed at 350 °C.

(d) The SPAS signals, the signature of vacancy-like defects that are not fully saturated, decrease in density during annealing. The density of positron traps is higher in the samples implanted with hydrogen first, especially at a depth about 400 nm.

Hydrogen is a very active element. During implantation, a large part of the implanted hydrogen ions react with the silicon atoms, dangling bonds or defects, and a diversity of H-related complexes are formed near the projected range. Under some conditions (e.g. after annealing at a high temperature), hydrogen atoms will be released from the H-related complexes and combine with each other to form molecular hydrogen. The hydrogen atom's diffusivity is very high in silicon even at room temperature, but most of the hydrogen present is combined in complexes and cannot move. H_2 molecules are also difficult to move in the silicon lattice.

Helium is an inert element. During implantation, helium atoms do not react with the silicon atoms, dangling bonds or defects. The implanted helium atoms stay near the projected range. The helium atom's diffusivity is much lower than that of a hydrogen atom; it stays where it was at room temperature, but at higher temperatures it also is movable.

Due to the great difference of the interaction with silicon atoms between the hydrogen and helium atoms, the defects introduced by them are also different. Hydrogen generally generates vacancies, interstitial atoms, bubbles, cracks and platelets, while helium introduces only vacancies, interstitial atoms and bubbles.

If there is enough hydrogen in the samples, the role of the implanted H is twofold. First, it acts chemically, in that it drives the formation of microscopically flat internal surfaces—platelets—and acts as a source of gaseous H_2 which becomes trapped in the internal cavities. Second, it acts physically, as an internal pressure source. Helium only acts physically as an internal pressure source. During hydrogen ion implantation extended defects, platelets and vacancies are generated. The inner surfaces of these extended defects are hydronized. Some of the Si–Si bonds are replaced by Si–H–H–Si bonds (one of the most important H-related complexes that cause exfoliation) which are much weaker than the Si–Si bonds [12]. During annealing, some of the H-related complex relapse, hydrogen atoms are released and combine with each other and molecular hydrogen is formed in the silicon crystal. The breaking of the hydrogen bond in Si–H–H–Si introduces platelets. During annealing at a higher temperature, the molecular H_2 and He atoms are movable. If the molecular H_2 and He atoms stay in the platelets, the free energy of the system is much lower than that when they stay in an interstitial place. So the molecular H_2 and the helium atoms are apt to accumulate in these extended defects, and exert great pressure on the inner surfaces of extended defects. The structure of a platelet is easier to split than other extended defects (such as bubbles) due to their mechanical and chemical structure. During annealing, more and more molecular H_2 and helium atoms are released from the lattice and accumulate in the platelets. The platelets become larger and larger under the influence of the inner pressure; finally, some of them connect with each other. The diameter of platelets is about several nanometres before annealing, and is about several tens of nanometres after annealing [5]. When the annealing temperature is above 400 °C, blistering and exfoliation occur. During the splitting process, platelets play a much more important role than the bubbles. Helium plays an important role in that process. First, helium will not combine with the silicon atoms and it moves slowly, so during annealing at a certain temperature it will not escape or be combined by a defect; as such it is much easier for helium than hydrogen to accumulate in the platelets. Second, helium is composed of single atoms rather than being molecular: it doubles the effect when implanted with the same dose as hydrogen.

It is clear that the initial distributions of helium and hydrogen in both implantation orders after implantation are similar. However, after annealing the distribution of hydrogen remains similar in the samples with the different implantation orders.

The distribution of helium is very different. In hydrogen-implanted-first samples, the helium atoms move to the hydrogen implantation region after annealing at 350 °C, while in the helium-implanted-first samples the helium atoms only move a little deeper. Helium contributes less in the platelet inner pressure during annealing in the helium-implanted-first samples.

Since the greatest amount of hydrogen and helium exists in the lattice after implantation, the interstitial gas atoms increase the free energy of the system, especially near the projected range. During annealing more and more silicon atoms are 'kicked out' into interstitial positions to decrease the free energy, and Frenkel pairs form. During annealing both types of gas atom are movable. Because of the lower free energy in the vacancies, gas atoms accumulate there. Therefore the interstitial silicon atoms (one kind of displacement atom) increase rapidly, which can be concluded from the result of RBS/C. Hydrogen combines with these vacancies and form VH_n [11]. The vacancies are filled by the gas atoms and are passivated, so that the vacancies lose the ability to trap positrons.

Compared with the helium-implanted-first samples, the density of interstitial atoms is lower and the density of positron traps is higher after annealing at 400 °C in the hydrogen-implanted-first samples. Therefore, it is concluded that in the helium-implanted-first samples the helium atoms cannot move to the hydrogen-distributed region, cannot move into the platelet and they stay in the lattice; therefore more gas molecules stay in the lattice and the free energy is higher than that in the hydrogen-implanted-first samples. So the helium atoms and hydrogen molecules introduce more vacancies and interstitial silicon atoms than in hydrogen-implanted-first samples. The vacancies are passivated by the gas molecules. In helium-implanted-first samples, more helium atoms are captured by the vacancies for they stay in the near lattice, not in the far away platelets. More vacancies—positron traps—are decorated by gas molecules in the helium-implanted-first samples. The density of positron traps is lower in the helium-implanted-first samples. Because fewer helium atoms are in the platelets, helium contributes less to the inner pressure of the platelets; the effect of exfoliation in the helium-implanted-first samples is less than that in the hydrogen-implanted-first samples. It is also confirmed by XTEM, in figures 4(a) and 4(b), that the density of platelets in the hydrogen-implanted-first samples are much higher. The reason why helium atoms in the helium-implanted-first samples cannot move to the hydrogen-distributed depth, just as they do in the hydrogen-implanted-first samples, is not clear.

5. Conclusions

The H and He coimplanted Si samples were characterized by XTEM, ERDA and RBS/C. We observed the synergistic effect when hydrogen and helium implantation is combined in different orders. The total implantation dose necessary for exfoliation is less than H or He only implantation. It is also found that there are some differences in the effect between the different orders of implantation. Compared with the helium-implanted-first samples, in the hydrogen-implanted-first samples the helium atoms move deeper, fewer interstitial silicon atoms are induced and fewer positron traps are passivated. It is not so efficient to exfoliate the surface in the samples implanted with helium first than in the samples implanted with hydrogen first.

Acknowledgments

This work is supported by the National 973 plan of China (No G200003), the National Natural Science Foundation of China (No 19775062 and No 69976034) and the Shanghai Youth Foundation (No 98JC14004).

References

[1] Wong-Leung J, Ascheron C E and Petravic M 1995 *Appl. Phys. Lett.* **66** 1231
[2] Wong-Leung J, Nygren E and Williams J S 1995 *Appl. Phys. Lett.* **67** 416
[3] Wong-Leung J *et al* 1995 *Nucl. Instrum. Methods* B **96** 253
[4] Bruel M 1995 *Electron. Lett.* **31** 1201
[5] Weldon M K *et al* 1997 *J. Vac. Sci. Technol.* B **15** 1065
[6] Agarwal A, Haynes T E, Venezia V C, Holland O W and Eaglesham D J 1998 *Appl. Phys. Lett.* **72** 1086
[7] Corni F *et al* 1999 *J. Appl. Phys.* **85** 1401
[8] Brusa R S, Karwasz G P, Tiengo N, Zecca A, Corni F, Calzolari G and Nobili C 1999 *J. Appl. Phys.* **85** 2390
[9] Cerofolini G F *et al* 1995 *Phys. Status Solidi* a **150** 539
[10] Brusa R S, Duarte Naia M, Zecca A, Nobili C, Ottaviani G, Tonini R and Dupasquier A 1994 *Phys. Rev.* B **49** 7271
[11] Weldon M K, Collot M, Chabal Y J, Venezia V C, Agarwal A, Haynes T E, Eaglesham D J, Christman S B and Chaban E E 1998 *Appl. Phys. Lett.* **73** 3721
[12] Pearton S J, Corbett J W and Stavola M 1992 *Hydrogen in Crystalline Semiconductors* (Berlin: Springer) and references therein
[13] Cerofolini G F, Meda L, Balboni R, Corni F, Frabboni S, Ottaviani G, Tonini R, Anderle M and Canteri R 1992 *Phys. Rev.* B **46** 2061